Progress In Electromagnetics Research, Vol. 110, 237–252, 2010

ON THE IMAGING OF THIN DIELECTRIC INCLUSIONS VIA TOPOLOGICAL DERIVATIVE CONCEPT

W. K. Park

Department of Mathematics
Kookmin University, Seoul 136-702, Korea

Abstract—In this paper, we consider the imaging of thin dielectric inclusions completed embedded in the homogeneous domain. To image such inclusion from boundary measurements, topological derivation concept is adopted. For that purpose, an asymptotic expansion of the boundary perturbations that are due to the presence of a small inclusion is considered. Applying this formula, we can design only one iteration procedure for imaging of thin inclusions by means of solving adjoint problem. Various numerical experiments without and with some noise show how the proposed techniques behave.

1. INTRODUCTION

There exists a considerable amount of interesting inverse problems concerned with the retrieval of inhomogeneities embedded in a homogeneous medium. Among them, One of the many interests in inverse problem is the non-destructive evaluation of electromagnetic inhomogeneities embedded in known media using high/low frequency time-harmonic electromagnetic propagation arising in physics [1, 3, 4, 6, 8, 11, 15, 16, 21, 30], medical science [2, 9, 14, 20, 32, 33], material engineering [12, 22], and so on. In order to retrieve such inhomogeneities, various algorithms have been developed. However, most of which are based on on least-square algorithms and Newton-type iteration schemes so that for a successful application of such schemes, one needs a good initial guess close enough to the unknown object. Without it, one might suffer from large computational costs with the risk of non convergence. Moreover, such schemes require not only suitable regularization terms depending upon the specific problem at hand but also complex calculation of so called Fréchet derivatives at each iteration step.

Received 13 October 2010, Accepted 11 November 2010, Scheduled 20 November 2010
Corresponding author: Won-Kwang Park (parkwk@kookmin.ac.kr).

In order to overcome such difficulties, alternative non-iterative imaging algorithm has suggested, for example, Linear sampling method [10, 13, 19], MUSIC (MUltiple SIgnal Classification)-type algorithm [3, 5, 18, 26, 27] and multi-frequency method [24, 25]. It has shown that these algorithms are fast, effective and robust. Moreover, they can be easily extended to the multiple inclusions. Unfortunately, for a successful application of such algorithms, a large amount of incident fields with various directions and corresponding scattered fields are required. Therefore, development a non-iterative imaging algorithm with a small amount of such fields is required.

In this paper, we develop a non-iterative imaging method of thin dielectric inclusion via the scattered field measured at boundary induced from a small number of incident field. For that purpose the topological derivative concept is adopted. Notice that in the field of shape optimization, a topological derivative is a derivative of a function of a region with respect to small changes in its topology, such as adding a small inclusion and so on. For that purpose, we will apply the asymptotic expansion formula due to the presence of small dielectric inclusion to express the integral equation of topological derivative and to design and solve the adjoint problems.

Let us signal that sometimes poor results appeared via non-iterative method so that they could not guarantee the complete shape of thin inclusions (see Figures 6, 7 and examples in [5, 18, 20, 26, 27]). However, once the results are obtained, one could apply them to the traditional iterative algorithm to retrieve a better shape once an appropriate cost functional is chosen (see [28] for instance).

This paper structured as follows. Two-dimensional electromagnetic scattering from a dielectric thin inclusion and asymptotic expansion formula due to the presence of small inclusion is introduced in Section 2. In Section 3, we derive the topological derivatives by means of an adjoint technique. In Section 4, we present various numerical experiments for demonstrating the performance of the proposed algorithm. A short conclusion appears in Section 5.

2. THE DIRECT SCATTERING PROBLEM & ASYMPTOTIC EXPANSION FORMULA

Let us consider two-dimensional electromagnetic scattering from a thin, curve-like homogeneous inclusion within a homogeneous domain Ω. Throughout this paper, we only consider only a dielectric contrast case and carry out the study in the two-dimensional Transverse Magnetic (TM) polarization. Assume that this domain Ω contains an inclusion denoted as Γ which is localized in the neighborhood of a curve σ. That

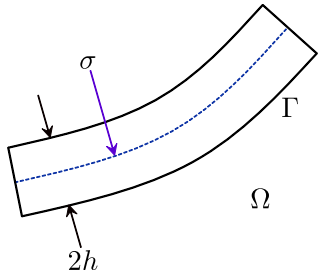

Figure 1. Sketch of the thin inclusion Γ with its supporting curve σ.

is,

$$\Gamma = \{x + \eta n(x) : x \in \sigma,\ \eta \in (-h, h)\}, \tag{1}$$

where the supporting σ is a simple, smooth curve completely embedded in Ω, $n(x)$ is the unit normal to σ at x, and h is a strictly positive constant which specifies the thickness of the inclusion (small with respect to the wavelength), refer to Figure 1.

Assume that every materials are fully characterized by their dielectric permittivity at a given frequency ω. Let $0 < \varepsilon_0 < +\infty$ and $0 < \varepsilon_T < +\infty$ denote the permittivity of the domain Ω and thin inclusion Γ, respectively. Then, one can define the piecewise constant dielectric permittivity

$$\hat{\varepsilon}(x) = \begin{cases} \varepsilon_0 & \text{for} \quad x \in \Omega \backslash \overline{\Gamma} \\ \varepsilon_T & \text{for} \quad x \in \Gamma. \end{cases} \tag{2}$$

In order to derive the topological derivative in Section 3, we need an asymptotic expansion formula due to the existence of small inclusion. Assume that Ω contains a small inclusion $\Sigma := z + rB$, where r is a small, real positive constant which specifies the magnitude of the diameter of Σ, B is a bounded, smooth domain (here, we assume that B is a disk) containing the origin, and z denotes the location such inclusion. Similarly with the Equation (2), let us define the piecewise constant dielectric permittivity

$$\varepsilon(x) = \begin{cases} \varepsilon_0 & \text{for} \quad x \in \Omega \backslash \overline{\Sigma} \\ \varepsilon & \text{for} \quad x \in \Sigma. \end{cases} \tag{3}$$

Let $u(x)$ and $v(x)$ be the time-harmonic total field which satisfies the Helmholtz equation in the presence of small inclusion Σ:

$$\begin{cases} \triangle u(x) + \omega^2 \varepsilon(x) u(x) = 0 & \text{in} \quad \mathbb{R}^2 \\ \dfrac{\partial u}{\partial \nu}(x) = g(x) & \text{on} \quad \partial\Omega \end{cases} \tag{4}$$

and

$$\begin{cases} \triangle v(x) + \omega^2 \varepsilon(x) v(x) = 0 & \text{in} \quad \mathbb{R}^2 \\ v(x) = f(x) & \text{on} \quad \partial\Omega. \end{cases} \tag{5}$$

and let $u_0(x)$ and $v_0(x)$ be the solution of Equations (4) and (5) in the absence of such inclusion. Then asymptotic expansion formula in the presence of small inhomogeneity Σ can be written as (see [4])

$$u(x) - u_0(x) = r^2 \omega^2 (\varepsilon - \varepsilon_0)|B| u_0(z) \mathcal{N}(x, z) + o(r^2) \tag{6}$$

and

$$\frac{\partial v}{\partial \nu}(x) - \frac{\partial v_0}{\partial \nu}(x) = r^2 \omega^2 (\varepsilon - \varepsilon_0)|B| u_0(z) \frac{\partial \mathcal{G}(x, z)}{\partial \nu(x)} + o\left(r^2\right), \tag{7}$$

where $o(r^2)$ is uniform in $z \in \Sigma$, $\mathcal{N}$ and $\mathcal{G}$ be the Neumann and Dirichlet functions, respectively, the solution to

$$\begin{cases} \triangle \mathcal{N}(x, y) + \omega^2 \varepsilon_0 \mathcal{N}(x, y) = -\delta(x, y) & \text{in} \quad \Omega \\ \dfrac{\partial \mathcal{N}(x, y)}{\partial \nu(x)} = 0 & \text{on} \quad \partial\Omega \end{cases}$$

and

$$\begin{cases} \triangle \mathcal{G}(x, y) + \omega^2 \varepsilon_0 \mathcal{G}(x, y) = \delta(x, y) & \text{in} \quad \Omega \\ \mathcal{G}(x, y) = 0 & \text{on} \quad \partial\Omega. \end{cases}$$

3. DERIVATION OF TOPOLOGICAL DERIVATIVE

The topological derivative measures the influence of creating a small inclusion at a certain point inside the domain Ω. Mathematically speaking, the topological derivative $d_T \mathcal{J}(z)$ of a function $\mathcal{J}(\Omega)$ at a point z inside Ω can be defined by

$$\mathcal{J}(\Omega \backslash \Sigma) = \mathcal{J}(\Omega) + \rho(r) d_T \mathcal{J}(z) + o(\rho(r)),$$

where Σ is a small ball(inclusion) of small radius r placed at z and the function $\rho(r) \longrightarrow 0$ as $r \longrightarrow 0$. See [5, 6, 16, 17, 31] for instance.

Suppose that Ω contains a thin inclusion Γ and let $g^{(l)}(x)$, $l = 1, 2, \ldots, N$, be N given functions denote the boundary condition on $\partial\Omega$. The problem we consider in this paper is to construct an image of Γ from the boundary measurements $u_\Gamma^{(l)}(x)$ for $x \in \partial\Omega$, where the function $u_\Gamma^{(l)}$ for $l = 1, 2, \ldots, N$, is the solution to

$$\begin{cases} \triangle u_\Gamma^{(l)}(x) + \omega^2 \hat{\varepsilon}(x) u_\Gamma^{(l)}(x) = 0 & \text{in} \quad \Omega \\ \dfrac{\partial u_\Gamma^{(l)}}{\partial \nu}(x) = g^{(l)}(x) & \text{on} \quad \partial\Omega, \end{cases} \tag{8}$$

where $\hat{\varepsilon}(x)$ is defined in Equation (2). With this, let us construct $u_N^{(l)}$ and $u_D^{(l)}$ as the solutions to the following problems in the absence of inclusion:

$$\begin{cases} \triangle u_D^{(l)}(x) + \omega^2 \varepsilon_0 u_D^{(l)}(x) = 0 & \text{in} \quad \Omega \\ u_D^{(l)}(x) = u_\Gamma^{(l)}(x) & \text{on} \quad \partial\Omega \end{cases} \tag{9}$$

and

$$\begin{cases} \triangle u_N^{(l)}(x) + \omega^2 \varepsilon_0 u_N^{(l)}(x) = 0 & \text{in} \quad \Omega \\ \dfrac{\partial u_N^{(l)}}{\partial \nu}(x) = g^{(l)}(x) & \text{on} \quad \partial\Omega, \end{cases} \tag{10}$$

respectively. Then we can define the following discrepancy function:

$$\mathcal{J}(\Omega) := \frac{1}{2} \sum_{l=1}^{N} \int_{\partial\Omega} \left(\left| \frac{\partial u_D^{(l)}}{\partial \nu}(x) - g^{(l)}(x) \right|^2 + \left| u_N^{(l)}(x) - u_\Gamma^{(l)}(x) \right|^2 \right) dS(x). \tag{11}$$

Now, we can obtain the following result:

Theorem 3.1 *Let us denote Ref be the real part of f. Then the topological derivative $d_T\mathcal{J}(z)$ of the discrepancy function $\mathcal{J}(\Omega)$ satisfies*

$$\mathcal{J}(\Omega \backslash \Sigma) = \mathcal{J}(\Omega) + r^2 \omega^2 (\varepsilon - \varepsilon_0) |B| d_T \mathcal{J}(z) + o(r^2),$$

where

$$d_T \mathcal{J}(z) = \mathrm{Re} \sum_{l=1}^{N} \left(v_D^{(l)}(z) \overline{u_D^{(l)}(z)} + v_N^{(l)}(z) \overline{u_N^{(l)}(z)} \right), \tag{12}$$

and the adjoint states $v_D^{(l)}(z)$ and $v_N^{(l)}(z)$ are defined as the solution to

$$\begin{cases} \triangle v_D^{(l)}(x) + \omega^2 \varepsilon_0 v_D^{(l)}(x) = 0 & \text{in} \quad \Omega \\ v_D^{(l)}(x) = \dfrac{\partial u_D^{(l)}}{\partial \nu}(x) - g^{(l)}(x) & \text{on} \quad \partial\Omega \end{cases} \tag{13}$$

and

$$\begin{cases} \triangle v_N^{(l)}(x) + \omega^2 \varepsilon_0 v_N^{(l)}(x) = 0 & \text{in} \quad \Omega \\ \dfrac{\partial v_N^{(l)}}{\partial \nu}(x) = u_N^{(l)}(x) - u_\Gamma^{(l)}(x) & \text{on} \quad \partial\Omega. \end{cases} \tag{14}$$

Proof. In order to derive the topological derivative, let us create a small inclusion $\Sigma := z + rB$ at a certain point z inside the domain Ω

and denote $u_{D,\Sigma}^{(l)}$ and $u_{N,\Sigma}^{(l)}$ be the solutions of the following problems in the presence of Σ:

$$\begin{cases} \triangle u_{D,\Sigma}^{(l)}(x) + \omega^2 \varepsilon(x) u_{D,\Sigma}^{(l)}(x) = 0 & \text{in} \quad \Omega \\ u_{D,\Sigma}^{(l)}(x) = u_{\Gamma}^{(l)}(x) & \text{on} \quad \partial\Omega \end{cases} \tag{15}$$

and

$$\begin{cases} \triangle u_{N,\Sigma}^{(l)}(x) + \omega^2 \varepsilon(x) u_{N,\Sigma}^{(l)}(x) = 0 & \text{in} \quad \Omega \\ \dfrac{\partial u_{N,\Sigma}^{(l)}}{\partial \nu}(x) = g^{(l)}(x) & \text{on} \quad \partial\Omega, \end{cases} \tag{16}$$

respectively.

Applying equations (6) and (7), we can compute $\mathcal{J}(\Omega\backslash\Sigma)$ and examine the relationship between $\mathcal{J}(\Omega\backslash\Sigma)$ and $\mathcal{J}(\Omega)$ as follows:

$$\begin{aligned} &\mathcal{J}(\Omega\backslash\Sigma) \\ =&\frac{1}{2}\sum_{l=1}^{N}\int_{\partial\Omega}\left(\left|\frac{\partial u_{D,\Sigma}^{(l)}}{\partial\nu}(x) - g^{(l)}(x)\right|^2 + \left|u_{N,\Sigma}^{(l)}(x) - u_{\Gamma}^{(l)}(x)\right|^2\right) dS(x) \\ =&\frac{1}{2}\sum_{l=1}^{N}\int_{\partial\Omega}\left(\left|\frac{\partial u_{D}^{(l)}}{\partial\nu}(x) - g^{(l)}(x)\right|^2 + \left|u_{N}^{(l)}(x) - u_{\Gamma}^{(l)}(x)\right|^2\right) dS(x) \\ &+\sum_{l=1}^{N}\int_{\partial\Omega}\left(\frac{\partial u_{D}^{(l)}}{\partial\nu}(x) - g^{(l)}(x)\right)\left(\overline{\frac{\partial u_{D,\Sigma}^{(l)}}{\partial\nu}(x) - \frac{\partial u_{D}^{(l)}}{\partial\nu}(x)}\right) dS(x) \\ &+\sum_{l=1}^{N}\int_{\partial\Omega}\left(u_{N}^{(l)}(x) - u_{\Gamma}^{(l)}(x)\right)\left(\overline{u_{N,\Sigma}^{(l)}(x) - u_{N}^{(l)}(x)}\right) dS(x) + o(r^2) \\ =&\mathcal{J}(\Omega) + \mathcal{J}_D(z) + \mathcal{J}_N(z) + o\left(r^2\right), \end{aligned} \tag{17}$$

where

$$\mathcal{J}_D(z) = \sum_{l=1}^{N}\int_{\partial\Omega}\left(\frac{\partial u_{D}^{(l)}}{\partial\nu}(x) - g^{(l)}(x)\right)\left(\overline{\frac{\partial u_{D,\Sigma}^{(l)}}{\partial\nu}(x) - \frac{\partial u_{D}^{(l)}}{\partial\nu}(x)}\right) dS(x)$$

and

$$\mathcal{J}_N(z) = \sum_{l=1}^{N}\int_{\partial\Omega}\left(u_{N}^{(l)}(x) - u_{\Gamma}^{(l)}(x)\right)\left(\overline{u_{N,\Sigma}^{(l)}(x) - u_{N}^{(l)}(x)}\right) dS(x).$$

Therefore, topological derivative $d_T\mathcal{J}(z)$ can be obtained via evaluation of $\mathcal{J}_D(z)$ and $\mathcal{J}_N(z)$.

First, applying asymptotic expansion formula in Equation (7) and boundary condition in Equation (13), $\mathcal{J}_D(z)$ can be written

$$\begin{aligned}\mathcal{J}_D(z) =& \sum_{l=1}^{N}\int_{\partial\Omega}\left(\frac{\partial u_D^{(l)}}{\partial\nu}(x)-g^{(l)}(x)\right)\overline{\left(\frac{\partial u_{D,\Sigma}^{(l)}}{\partial\nu}(x)-\frac{\partial u_D^{(l)}}{\partial\nu}(x)\right)}dS(x)\\ =& \sum_{l=1}^{N}\int_{\partial\Omega} v_D^{(l)}(x)\overline{\left(\frac{\partial u_{D,\Sigma}^{(l)}}{\partial\nu}(x)-\frac{\partial u_D^{(l)}}{\partial\nu}(x)\right)}dS(x)\\ =& r^2\omega^2(\varepsilon-\varepsilon_0)|B|\sum_{l=1}^{N}\int_{\partial\Omega} v_D^{(l)}(x)\overline{u_D^{(l)}(z)\frac{\partial G(x,z)}{\partial\nu(x)}}dS(x).\end{aligned}$$

Then applying integration by parts yields

$$\begin{aligned}&\int_{\partial\Omega} v_D^{(l)}(x)\overline{u_D^{(l)}(z)\frac{\partial G(x,z)}{\partial\nu(x)}}dS(x)\\ =&\int_{\Omega}\left[v_D^{(l)}(x)\overline{u_D^{(l)}(z)\triangle G(x,z)}+\nabla v_D^{(l)}(x)\cdot\left(\overline{u_D^{(l)}(z)\nabla G(x,z)}\right)\right]dx\\ =&\int_{\Omega}\left[v_D^{(l)}(x)\overline{u_D^{(l)}(z)\triangle G(x,z)}+v_D^{(l)}(x)\overline{u_D^{(l)}(z)\omega^2\varepsilon_0 G(x,z)}\right]dx\\ &-\int_{\Omega}\left[\triangle v_D^{(l)}(x)\overline{u_D^{(l)}(z)G(x,z)}+v_D^{(l)}(x)\overline{u_D^{(l)}(z)\omega^2\varepsilon_0 G(x,z)}\right]dx\\ =&\int_{\Omega}\left[v_D^{(l)}(x)\overline{u_D^{(l)}(z)\left(\triangle G(x,z)+\omega^2\varepsilon_0 G(x,z)\right)}\right]dx\\ &-\int_{\Omega}\left[\left(\triangle v_D^{(l)}(x)+\omega^2\varepsilon_0 v_D^{(l)}(x)\right)\overline{u_D^{(l)}(z)G(x,z)}\right]dx\\ =&v_D^{(l)}(z)\overline{u_D^{(l)}(z)}\end{aligned}\tag{18}$$

for all $l=1,2,\ldots,N$. Therefore, we can obtain

$$\mathcal{J}_D(z)=r^2\omega^2(\varepsilon-\varepsilon_0)|B|\sum_{l=1}^{N}v_D^{(l)}(z)\overline{u_D^{(l)}(z)}.\tag{19}$$

Next, applying asymptotic expansion formula in Equation (6) and

boundary condition in Equation (14) yields

$$\begin{aligned}\mathcal{J}_N(z) &= \sum_{l=1}^{N} \int_{\partial\Omega} \left(u_N^{(l)}(x) - u_\Gamma^{(l)}(x)\right) \left(\overline{u_{N,\Sigma}^{(l)}(x) - u_N^{(l)}(x)}\right) dS(x) \\ &= \sum_{l=1}^{N} \int_{\partial\Omega} \frac{\partial v_N^{(l)}}{\partial \nu}(x) \left(\overline{u_{N,\Sigma}^{(l)}(x) - u_N^{(l)}(x)}\right) dS(x) \\ &= r^2\omega^2(\varepsilon - \varepsilon_0)|B| \sum_{l=1}^{N} \int_{\partial\Omega} \frac{\partial v_N^{(l)}}{\partial \nu}(x) \overline{u_N^{(l)}(z)\mathcal{N}(x,z)} dS(x).\end{aligned}$$

Then integration by parts yields

$$\begin{aligned}&\int_{\partial\Omega} \frac{\partial v_N^{(l)}}{\partial \nu}(x) \overline{u_N^{(l)}(z)\mathcal{N}(x,z)} dS(x) \\ =&\int_\Omega \left[\triangle v_N^{(l)}(x) \overline{u_N^{(l)}(z)\mathcal{N}(x,z)} + \nabla v_N^{(l)}(x) \cdot \overline{u_N^{(l)}(z)\nabla\mathcal{N}(x,z)}\right] dx \\ =&\int_\Omega \left[\triangle v_N^{(l)}(x) \overline{u_N^{(l)}(z)\mathcal{N}(x,z)} + \omega^2\varepsilon_0 v_N^{(l)}(x) \overline{u_N^{(l)}(z)\mathcal{N}(x,z)}\right] dx \\ &- \int_\Omega \left[v_N^{(l)}(x) \overline{u_N^{(l)}(z)\triangle\mathcal{N}(x,z)} + \omega^2\varepsilon_0 v_N^{(l)}(x) \overline{u_N^{(l)}(z)\mathcal{N}(x,z)}\right] dx \\ =&\int_\Omega \left[\left(\triangle v_N^{(l)}(x) + \omega^2\varepsilon_0 v_N^{(l)}(x)\right) \overline{u_N^{(l)}(z)\mathcal{N}(x,z)}\right] dx \\ &- \int_\Omega \left[v_N^{(l)}(x) \overline{u_N^{(l)}(z)\left(\triangle\mathcal{N}(x,z) + \omega^2\varepsilon_0\mathcal{N}(x,z)\right)}\right] dx \\ =&v_N^{(l)}(z)\overline{u_N^{(l)}(z)}. \end{aligned} \tag{20}$$

for all $l = 1, 2, \ldots, N$. Therefore, we can obtain

$$\mathcal{J}_N(z) = r^2\omega^2(\varepsilon - \varepsilon_0)|B| \sum_{l=1}^{N} v_N^{(l)}(z)\overline{u_N^{(l)}(z)}. \tag{21}$$

Finally, by taking real parts of sum of Equations (19) and (21), we can obtain Equation (12).

The points where the topological derivative is the most negative are expected to be approximately on σ so that this would yields a shape of Γ. Roughly speaking, inserting small ball in the most negative gradient regions minimizes the discrepancy between the boundary measurements $u_\Gamma^{(l)}$ and the solutions in the presence of these balls with the Neumann data $g^{(l)}$ for $l = 1, 2, \ldots, N$. It is worth mentioning that the negative gradient regions are obtained in only one iteration so that this method will be faster than the traditional iterative method.

4. NUMERICAL EXPERIMENTS

In this section, we present results of numerical simulations using the evaluation of topological derivative $d_T\mathcal{J}(z)$ we derived in the previous subsections to image thin dielectric inclusions. For that purpose, we choose the homogeneous domain Ω as a unit circle centered at the origin in $\mathbb{R}^2$ and three thin inclusions Γ_j are chosen for illustration:

$$\Gamma_j = \{x + \eta n(x) : x \in \sigma_j,\ \eta \in (-h, h)\},$$

with symmetric, non-symmetric and oscillating supporting curves σ_1, σ_2 and σ_3, respectively, represented as

$$\begin{aligned}
\sigma_1 &= \left\{(s - 0.2, -0.5s^2 + 0.5) : s \in [-0.5, 0.5]\right\} \\
\sigma_2 &= \left\{(s + 0.2, s^3 + s^2 - 0.6) : s \in [-0.5, 0.5]\right\} \\
\sigma_3 &= \left\{(s, 0.5s^2 + 0.1\sin(3\pi(z + 0.7))) : s \in [-0.7, 0.7]\right\}.
\end{aligned} \tag{22}$$

and we denote ε_j be the permittivities of Γ_j. The thickness h of thin inclusions Γ_j is set to 0.02 and permittivity ε_0 of domain Ω is chosen as 1. Since ε_0 are set to unity, the applied frequency reads as $\omega = \frac{2\pi}{\lambda}$, at wavelength λ, i.e., the boundary conditions in Equations (8) and (10) can be read as

$$g^{(l)}(x) := \frac{\partial u}{\partial \nu}(x) = \frac{\partial e^{i\omega\theta_l \cdot x}}{\partial \nu(x)} = i\omega\theta_l \cdot \nu(x) e^{i\omega\theta_l \cdot x}$$

for every $x \in \partial\Omega$ if we consider the plane wave illumination. We choose $N = 4$ different incident directions

$$\theta_l := \left(\cos\frac{2l\pi}{N}, \sin\frac{2l\pi}{N}\right) \quad \text{for} \quad l = 1, 2, \ldots, N,$$

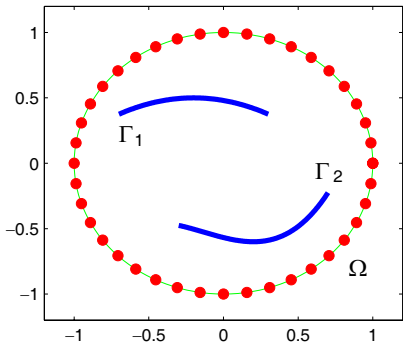

Figure 2. Sketch of the test configuration.

and have the measured data at $M = 40$ equidistant points x_m on $\partial\Omega$ (see Figure 2),

$$x_m := \left(\cos\frac{2m\pi}{M}, \sin\frac{2m\pi}{M}\right) \quad \text{for} \quad m = 1, 2, \ldots, M.$$

Let us emphasize that the forward problems in Equations (8), (9), (10), (13) and (14) are solved by Finite Element Method (FEM) in order to avoid the inverse crime. Alternatively, one can employ an asymptotic formulation involving the solution of a second-kind Fredholm integral equation [23] and asymptotic expansion formula [7] along the supporting curve. See [27] for a detailed discussion of generating data and corresponding results.

For the first example, let us consider the imaging of Γ_1 with $\varepsilon_1 = 5$. Figure 3 is the plot of values of $d_T\mathcal{J}(z)$ for all $z \in \Omega$ at operating wavelength $\lambda = 0.5$. In this example, one can easily notice

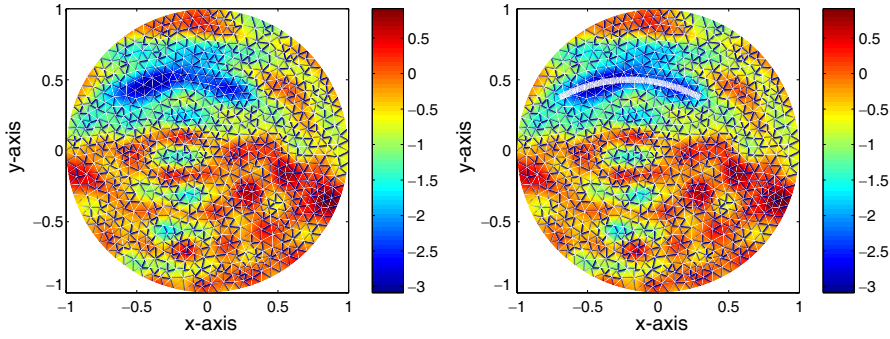

Figure 3. Map of $d_T\mathcal{J}(z)$ for $\lambda = 0.5$, without noise. White colored line is the Γ_1.

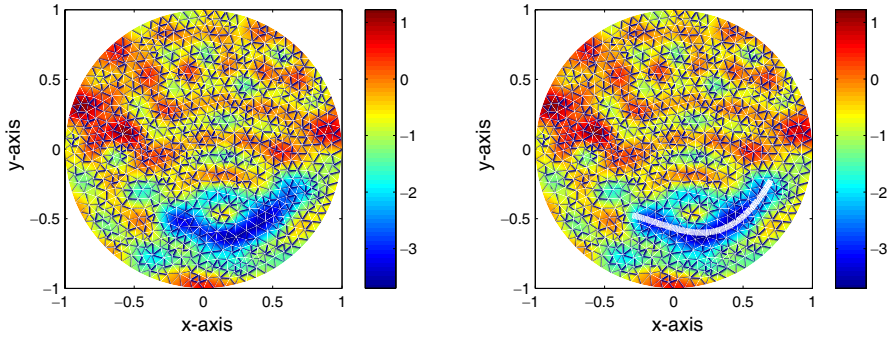

Figure 4. Map of $d_T\mathcal{J}(z)$ for $\lambda = 0.5$, without noise. White colored line is the Γ_2.

that the points where the topological derivative is the most negative value appears in the neighborhood of σ_1 so that and it provides a good initial guess.

Next, Figure 4 shows the plot of values of $d_T\mathcal{J}(z)$ when the thin inclusion is Γ_2 with $\varepsilon_2 = 5$ and operating wavelength $\lambda = 0.5$. In harmony with the previous example, good image of Γ_2 has appeared.

Let us apply this algorithm to an oscillating thin inclusion Γ_3. Typical result is illustrated in Figure 5 with $\varepsilon_3 = 5$ and operating wavelength $\lambda = 0.5$. By comparing with the result in [26, 27] the result is coarse so that an implementation is expected.

Both mathematical setting, derivation of topological derivative and numerical analysis could be extended in rather straightforward fashion to the case of multiple inclusions with same thickness h. Detailed derivation will not be considered herein, only examples are illustrated. For that purpose, let us consider the imaging of multiple inclusions $\Gamma_{\text{Multi}} = \Gamma_1 \cup \Gamma_2$ in Figures 6 and 7. By comparing with the

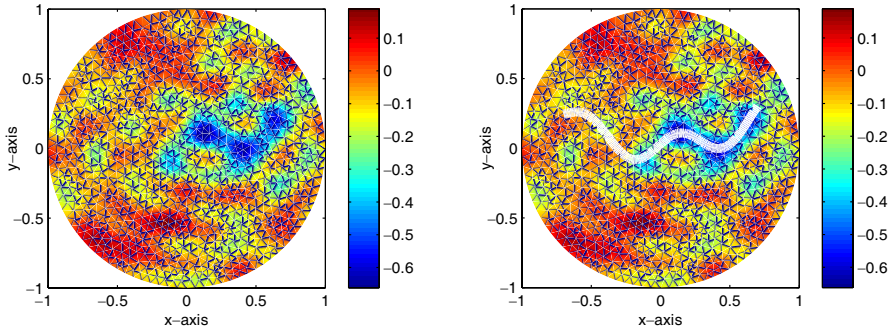

Figure 5. Map of $d_T\mathcal{J}(z)$ for $\lambda = 0.5$, without noise. White colored line is the Γ_3.

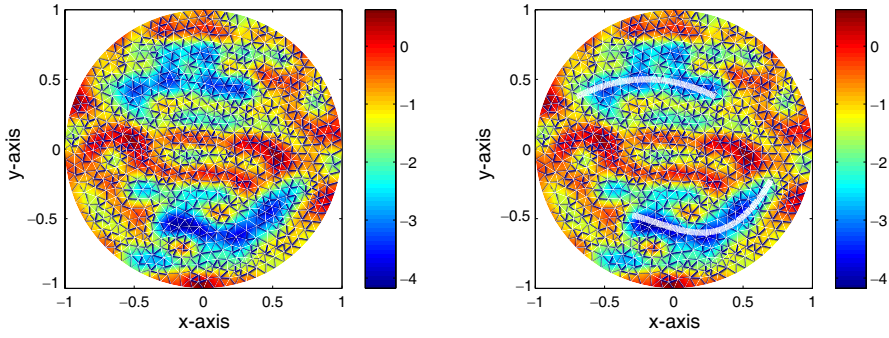

Figure 6. Map of $d_T\mathcal{J}(z)$ for $\lambda = 0.5$, without noise. White colored line is the Γ_{Multi} with same permittivities.

single inclusion cases, refer to Figures 3 and 4, we can easily recognize the existence of such inclusions. It is interesting to observe that if an inclusion Γ_2 has a much smaller value of permittivity than the other Γ_1, say $\varepsilon_1 = 10$ and $\varepsilon_2 = 5$, this inclusion does not significantly affect the scattered field so that it appeared with much smaller magnitude than the other one, refer to Figure 7. As we mentioned in the introduction, although obtained results are poor, such results of low computational cost could provide initial guesses of the traditional Newton-type based algorithm or of a level-set evolution [1, 16, 28, 29].

In order to show the robustness of proposed algorithm, we added a white Gaussian noise with 20 dB signal-to-noise ratio (SNR) to the measured boundary data $u_\Gamma^{(l)}(x)$ in Equation (8). Figures 8 and 9 illustrate the results when we add Gaussian noise for Γ_2 and Γ_{Multi}. By comparing with Figures 4 and 7, we can notice that proposed method is robust even under the presence of noise.

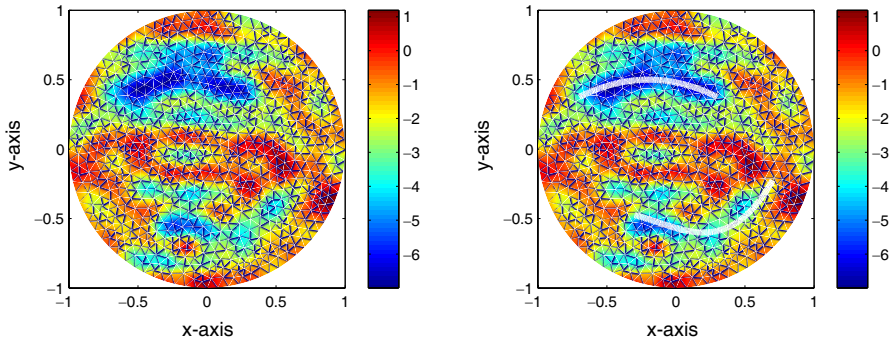

Figure 7. Map of $d_T\mathcal{J}(z)$ for $\lambda = 0.5$, without noise. White colored line is the Γ_{Multi} with different permittivities.

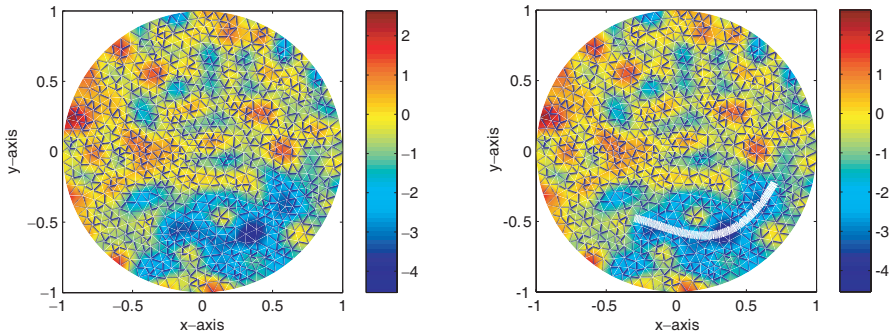

Figure 8. Map of $d_T\mathcal{J}(z)$ for $\lambda = 0.5$ in the presence of random noise when the thin inclusion is Γ_2.

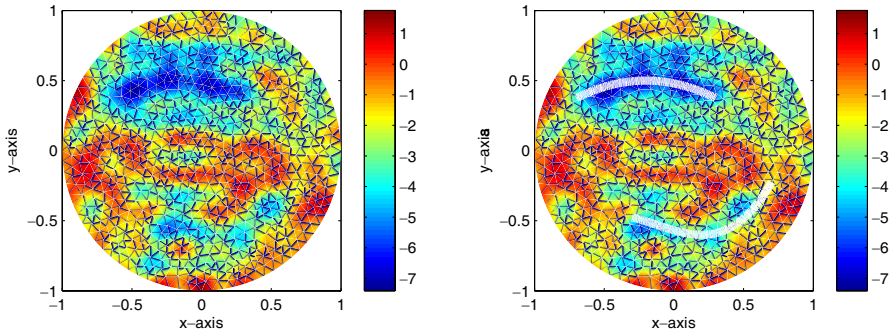

Figure 9. Map of $d_T\mathcal{J}(z)$ for $\lambda = 0.5$ in the presence of random noise when the thin inclusion is Γ_{Multi} with different permittivities.

5. CONCLUSION

Based on the topological derivative concept, a non-iterative algorithm has been investigated for imaging thin dielectric curve-like inclusions embedded in a homogeneous domain Ω. Results show that this approach is fast, effective and stable so that such results of low computational cost could provide initial guesses of the traditional Newton-type based algorithm or of a level-set evolution [1, 16, 28].

Although, we have considered dielectric case only, the analysis could be extended for a purely magnetic contrast between inclusions and embedding domain, and combination cases so that it can be carry out the study in the Transverse Electric (TE) polarization. Recently, the asymptotic expansion formula due to the presence of small perfectly conducting crack with Dirichlet boundary condition for imaging of extended one is developed. Extension of such algorithm for Neumann boundary condition case is also an interesting subject.

In this paper, we considered the imaging in the presence of random noise. Development of a fast and robust imaging algorithm in the presence of random inclusions will be a forthcoming work. Finally, we have been considering a two-dimensional problem. The strategy which is suggested, e.g., mathematical treatment of the asymptotic formula, imaging algorithm, etc., could be extended to the three-dimensional problem.

ACKNOWLEDGMENT

The author would like to acknowledge professor Habib Ammari, Dominique Lesselier and Jin Keun Seo. This work was done while the author was visiting the Department of Computational Science and Engineering in Yonsei University. This research was partially

supported by WCU(World Class University) program through the National Research Foundation of Korea(NRF) funded by the Ministry of Education, Science and Technology R31-2008-000-10049-0 and the research program 2010 of Kookmin University in Korea.

REFERENCES

1. Álvarez, D., O. Dorn, N. Irishina, and M. Moscoso, "Crack reconstruction using a level-set strategy," *J. Comput. Phys.*, Vol. 228, 5710–5721, 2009.
2. Ammari, H., *An Introduction to Mathematics of Emerging Biomedical Imaging*, Mathematics and Applications Series, Vol. 62, Springer-Verlag, Berlin, 2008.
3. Ammari, H., E. Iakovleva, and D. Lesselier, "A MUSIC algorithm for locating small inclusions buried in a half-space from the scattering amplitude at a fixed frequency," *SIAM Multiscale Modeling Simulation*, Vol. 3, 597–628, 2005.
4. Ammari, H. and H. Kang, *Reconstruction of Small Inhomogeneities from Boundary Measurements*, Lecture Notes in Mathematics, Vol. 1846, Springer-Verlag, Berlin, 2004.
5. Ammari, H., H. Kang, H. Lee, and W. K. Park, "Asymptotic imaging of perfectly conducting cracks," *SIAM J. Sci. Comput.*, Vol. 32, 894–922, 2010.
6. Auroux, D. and M. Masmoudi, "Image processing by topological asymptotic analysis," *ESAIM: Proc.*, Vol. 26, 24–44, 2009.
7. Beretta, E. and E. Francini, "Asymptotic formulas for perturbations of the electromagnetic fields in the presence of thin imperfections," *Contemp. Math.*, Vol. 333, 49–63, 2000.
8. Carpio, A. and M.-L. Rapun, "Solving inhomogeneous inverse problems by topological derivative methods," *Inverse Problems*, Vol. 24, 045014, 2008.
9. Chen, X., "Subspace-based optimization method in electric impedance tomography," *Journal of Electromagnetic Waves and Applications*, Vol. 23, No. 11–12, 1397–1406, 2009.
10. Cheney, M., "The linear sampling method and the MUSIC algorithm," *Inverse Problems*, Vol. 17, 591–595, 2001.
11. Cheng, X., B.-I. Wu, H. Chen, and J. A. Kong, "Imaging of objects through lossy layer with defects," *Progress In Electromagnetics Research*, Vol. 84, 11–26, 2008.
12. Chien, W., "Inverse scattering of an un-uniform conductivity scat-

terer buried in a three-layer structure," *Progress In Electromagnetics Research*, Vol. 82, 1–18, 2008.

13. Colton, D., H. Haddar, and P. Monk, "The linear sampling method for solving the electromagnetic inverse scattering problem," *SIAM J. Sci. Comput.*, Vol. 24, 719–731, 2002.
14. Conceicao, R. C., M. O'Halloran, M. Glavin, and E. Jones, "Comparison of planar and circular antenna configurations for breast cancer detection using microwave imaging," *Progress In Electromagnetics Research*, Vol. 99, 1–20, 2009.
15. Davy, M., J.-G. Minonzio, J. de Rosny, C. Prada, and M. Fink, "Influence of noise on subwavelength imaging of two close scatterers using time reversal method: theory and experiments," *Progress In Electromagnetics Research*, Vol. 98, 333–358, 2009.
16. Dorn, O. and D. Lesselier, "Level set methods for inverse scattering," *Inverse Problems*, Vol. 22, R67–R131, 2006.
17. Eschenauer, H. A., V. V. Kobelev, and A. Schumacher, "Bubble method for topology and shape optimization of structures," *Struct. Optim.*, Vol. 8, 42–51, 1994.
18. Hou, S., K. Sølna, and H. Zhao, "A direct imaging algorithm for extended targets," *Inverse Problems*, Vol. 22, 1151–1178, 2006.
19. Kirsch, A. and S. Ritter, "A linear sampling method for inverse scattering from an open arc," *Inverse Problems*, Vol. 16, 89–105, 2000.
20. Lee, H. and W. K. Park, "Location search algorithm of thin conductivity inclusions via boundary measurements," *ESAIM: Proc.*, Vol. 26, 217–229, 2009.
21. Lesselier, D. and B. Duchene, "Buried, 2-D penetrable objects illuminated by line sources: FFT-based iterative computations of the anomalous field," *Progress In Electromagnetic Research*, Vol. 5, 351–389, 1991.
22. Li, F., X. Chen, and K. Huang, "Microwave imaging a buried object by the GA and using the S11 parameter," *Progress In Electromagnetics Research*, Vol. 85, 289–302, 2008.
23. Nazarchuk, Z. and K. Kobayashi, "Mathematical modelling of electromagnetic scattering from a thin penetrable target," *Progress In Electromagnetic Research*, Vol. 55, 95–116, 2005.
24. Park, W. K., "Non-iterative imaging of thin electromagnetic inclusions from multi-frequency response matrix," *Progress In Electromagnetic Research*, Vol. 106, 225–241, 2010.
25. Park, W. K., "On the imaging of thin dielectric inclusions buried within a half-space," *Inverse Problems*, Vol. 26, 074008, 2010.

26. Park, W. K. and D. Lesselier, "Electromagnetic MUSIC-type imaging of perfectly conducting, arc-like cracks at single frequency," *J. Comput. Phys.*, Vol. 228, 8093–8111, 2009.
27. Park, W. K. and D. Lesselier, "MUSIC-type imaging of a thin penetrable inclusion from its far-field multi-static response matrix," *Inverse Problems*, Vol. 25, 075002, 2009.
28. Park, W. K. and D. Lesselier, "Reconstruction of thin electromagnetic inclusions by a level set method," *Inverse Problems*, Vol. 25, 085010, 2009.
29. Ramananjaona, C., M. Lambert, D. Lesselier, and J.-P. Zolé sio, "Shape reconstruction by controlled evolution of a level set: from a min-max formulation to numerical experimentation," *Inverse Problems*, Vol. 17, 1087–1111, 2001.
30. Raza, M. I. and R. E. DuBroff, "Detecting dissimilarities in EM constitutive parameters using differential imaging operator on reconstructed wavefield," *Progress In Electromagnetics Research*, Vol. 98, 267–282, 2009.
31. Sokolowski, J. and A. Zochowski, "On the topological derivative in shape optimization," *SIAM J. Control Optim.*, Vol. 37, No. 4, 1251–1272, 1999.
32. Soleimani, M., "Simultaneous reconstruction of permeability and conductivity in magnetic induction tomography," *Journal of Electromagnetic Waves and Applications*, Vol. 23, 785–798, 2009.
33. Zhou, H., T. Takenaka, J. E. Johnson, and T. Tanaka, "A breast imaging model using microwaves and a time domain three dimensional reconstruction method," *Progress In Electromagnetics Research*, Vol. 93, 57–70, 2009.